Centre for Geo-Information

Thesis Report GIRS-2015-05

Influence of Solar Geometry on the Enhanced Vegetation Index in Observations of an Unmanned Aerial Vehicle and the Ross-Li model

Benjamin Brede

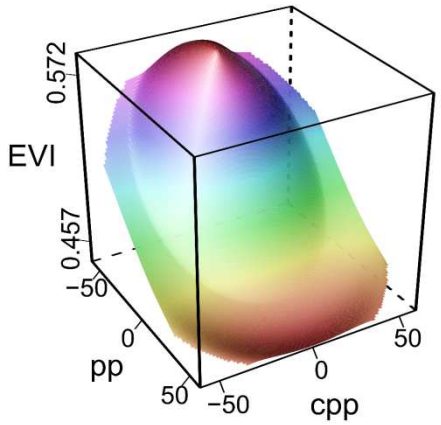

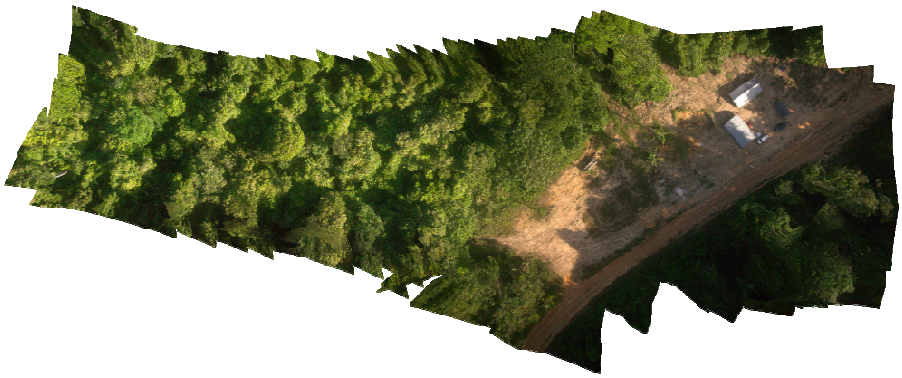

February 2015

WAGENINGEN UNIVERSITY
WAGENINGEN UR

Influence of Solar Geometry on the Enhanced Vegetation Index in Observations of an Unmanned Aerial Vehicle and the Ross-Li model

Benjamin Brede

Registration number 88 03 11 120 130

Supervisors:

Dr. Juha Suomalainen
Dr. Harm Bartholomeus

A thesis submitted in partial fulfilment of the degree of Master of Science
at Wageningen University and Research Centre,
The Netherlands.

February 16, 2014
Wageningen, The Netherlands

Thesis code number: GRS-80424
Thesis Report: GIRS-2015-05
Wageningen University and Research Centre
Laboratory of Geo-Information Science and Remote Sensing

Abstract

In this study the effect of solar geometry on Enhanced Vegetation Index (EVI) was studied. For this sub-crown resolution hyperspectral data of a Guyanese tropical rainforest has been collected with an Unmanned Aerial Vehicle (UAV) at 5 different solar zenith angles θ_s during one day. The hyperspectral data was used to simulate Moderate-Resolution Imaging Spectroradiometer (MODIS) spectral bands and generate EVI. The linear trend of EVI with θ_s at nadir viewing conditions was found to be -0.00285 $\frac{\Delta EVI}{\Delta \theta_s}$ ($p < 0.001$). A trend extracted from another study was about 40% stronger, but that study considered the intra-annual change of EVI which might have included an actual change in the canopy in the trend. Nonetheless, the influence of solar geometry on EVI was prevailing in both studies. Analysis of EVI images with sub-crown resolution pointed to strong influence of canopy shadows on EVI, which is supported by other studies. Therefore, EVI's dependence on solar geometry is mediated through shadowing effects, which in turn gives EVI the capability of detecting canopy structure. Additionally, the EVI-solar geometry relationship in the semi-empirical RossThick-LiSparse-Reciprocal (RTLSR) model was investigated. A database of model parameters of tropical forests has been extracted from the MODIS MCD43 product suite. For each RTLSR parameter set EVI was modeled with nadir viewing conditions and at different θ_s, and linear regressions were fit to represent the EVI-solar geometry relationship. The linear approximated EVI-solar geometry relationship was found to be -0.00149 $\frac{\Delta EVI}{\Delta \theta_s}$ on average, about 2 times weaker compared to the trend derived from the UAV. The reason for this might be the low differences in solar geometry during the sampling period of MODIS, which cause an under representation of solar geometry during the RTLSR model inversion. However, further analysis of the relationship between the single RTLSR model parameters and the EVI-solar geometry relationship showed that the RTLSR produces the trend for the right reason, namely canopy shadowing. In total this study delivers further evidence that EVI is dependent on solar geometry and this effect is mediated through EVI's sensitivity to within canopy shadows.

Keywords: Enhanced Vegetation Index, sun sensor geometry effects, Unmanned Aerial Vehicle, Moderate-Resolution Imaging Spectroradiometer, tropical forest

1 Introduction

Tropical rainforests contribute a substantial number to the global biodiversity hotspots and represent one of the largest terrestrial carbon pools (Lorenz and Lal, 2010). Satellite remote sensing is considered a suitable tool to monitor spatial and temporal changes in this ecosystem over large areas (Anderson, 2012). Recent studies of optical satellite data found a green-up of forest canopies at the end of the dry season (Huete et al., 2006; Xiao et al., 2006; Myneni et al., 2007; Samanta et al., 2012). This goes along with increased carbon uptake measured by eddy covariance towers, but opposite to patterns anticipated by vegetation models (Saleska et al., 2003; Huete et al., 2006). The explanation for the positive response is that trees benefit from increased irradiance due to less cloud cover by flushing new leaves. Prerequisite for this is sufficient water supply through deep roots (Nepstad et al., 1994).

Satellite-borne observations of leaf flush are generally based on Moderate-Resolution Imaging Spectroradiometer (MODIS) Enhanced Vegetation Index (EVI) (Huete et al., 2002). This index is deemed particularly suitable for tropical rainforests, because in contrast to Normalized Difference Vegetation Index (NDVI), which is frequently used in temperate ecoregions, EVI does not saturate over the dense canopies. However, recent studies report sun and view angle effects on the temporal EVI signal. Sims et al. (2011) investigated the dependence of EVI on sun sensor geometry in 3 forest sites in the eastern US. They found that EVI was strongly influenced by view angle and recommend that care must be taken of this effect. Galvão et al. (2011) studied MODIS and Hyperion/Earth Observing-1 (EO-1) images at different solar zenith angles (θ_s). At the end of the dry season, when θ_s was lowest, EVI was highest. Lower θ_s during the dry season would reduce shading within the canopy, thus increasing Near Infrared Reflectance (NIR) reflectance. Since EVI is strongly correlated to NIR reflectance, it would follow this pattern over the year. Moura et al. (2012) support these findings with their study of Multi-angle Imaging SpectroRadiometer (MISR) images. MISR with its 9 separate cameras is specifically designed to study view and illumination effects on reflectance signals. Together, these studies underline the need to take care of sun sensor geometry effects when using MODIS EVI.

Morton et al. (2014) do not only find solar geometry effects on the temporal EVI signal over Amazon tropical forests, they even question a general canopy green-up during the dry season. For that they apply their own correction for solar and viewing angle effects on MODIS reflectance data and derive EVI from the corrected reflectances. This challenges the theory of light limited net primary production of Amazon forests supported by previous remote sensing based studies (Huete et al., 2006; Xiao et al., 2006; Myneni et al., 2007; Samanta et al., 2012).

The MCD43 product suite is a MODIS standard product that offers an easily accessible opportunity to model surface reflectance at arbitrary solar and view angles and thereby correcting for the before mentioned effects. It is routinely produced along all other MODIS land products (Schaaf et al., 2002, 2011) and based on statistically fitting MODIS reflectance observations on a pixel basis to a semi-empirical Bidirectional Reflectance Distribution Function (BRDF) model, the RossThick-LiSparse-Reciprocal (RTLSR) model. The derived model parameters can be used to model reflectance at given view and solar zenith angle.

The kernel based RTLSR model consists of three terms, which each characterize different surface scattering processes (Lucht et al., 2000): the isotropic kernel describes Lambertian

reflectance, the volumetric kernel describes intra-crown volume scattering by leaves in the canopy and is sensitive to leaf optical properties and their spatial density, and the geometric kernel describes shadowing effects of canopy gaps or protrusions.

While the isotropic kernel is not dependent on sun and observation geometry, the volumetric and geometric kernels are functions of sun and viewing geometry. Additionally, the model is inverted for each band λ separately. Bidirectional Reflectance Factors (BRFs) are modeled as a linear combination of the kernels:

$$BRF\left(\theta_s, \theta_v, \phi, \lambda\right) = f_{iso}\left(\lambda\right) + f_{vol}\left(\lambda\right) K_{vol}\left(\theta_s, \theta_v, \phi, \lambda\right) + f_{geo}\left(\lambda\right) K_{geo}\left(\theta_s, \theta_v, \phi, \lambda\right) \tag{1.1}$$

where BRF is the Bidirectional Reflectance Factor at view zenith angle θ_v, solar zenith angle θ_s and relative azimuth angle between sensor and sun ϕ. The parameters f_{iso}, f_{vol} and f_{geo} represent reflectances (Roujean et al., 1992) and are scaled according to the kernel values K_{vol} and K_{geo}. The volumetric RossThick kernel K_{vol} assumes a dense leaf canopy (Roujean et al., 1992) . It models the canopy as a homogenous medium with randomly oriented facets. The kernel is written as (Strahler et al., 1999):

$$K_{vol}\left(\theta_s, \theta_v, \phi\right) = \frac{\left(\frac{\pi}{2} - \xi\right)\cos\xi + \sin\xi}{\cos\theta_s + \cos\theta_v} - \frac{\pi}{4} \tag{1.2}$$

with ξ the angle between sun and sensor, which is defined as

$$\cos\xi = \cos\theta_s \cos\theta_v + \sin\theta_s \sin\theta_v \cos\phi \tag{1.3}$$

The geometric, reciprocal LiSparse kernel K_{geo} assumes a sparse leaf canopy, i. e. non-overlapping shadows cast by randomly distributed objects. It is formulated as (Lucht et al., 2000; Strahler et al., 1999):

$$K_{geo}\left(\theta_s, \theta_v, \phi\right) = O\left(\theta_s, \theta_v, \phi\right) - \sec\theta_s^{'} - \sec\theta_v^{'} + \frac{1}{2}\left(1 + \cos\xi^{'}\right)\sec\theta_v^{'}\sec\theta_s^{'} \tag{1.4}$$

where

$$O\left(\theta_s, \theta_v, \phi\right) = \frac{1}{\pi}\left(t - \sin t\cos t\right)\left(\sec\theta_s^{'} + \sec\theta_v^{'}\right) \tag{1.5}$$

$$\cos t = \frac{h}{b}\frac{\sqrt{D^2 + \left(\tan\theta_s^{'}\tan\theta_v^{'}\sin\phi\right)^2}}{\sec\theta_s^{'} + \sec\theta_v^{'}} \tag{1.6}$$

$$D = \sqrt{\tan^2\theta_s^{'} + \tan^2\theta_v^{'} - 2\tan\theta_s^{'}\tan\theta_v^{'}\cos\phi} \tag{1.7}$$

$$\cos\xi^{'} = \cos\theta_s^{'}\cos\theta_v^{'} + \sin\theta_s^{'}\sin\theta_v^{'}\cos\phi \tag{1.8}$$

$$\theta_s^{'} = \tan^{-1}\left(\frac{b}{r}\tan\theta_s\right),\ \theta_v^{'} = \tan^{-1}\left(\frac{b}{r}\tan\theta_v\right) \tag{1.9}$$

$$\sec\theta = \frac{1}{\cos\theta} \tag{1.10}$$

For MODIS processing the dimensionless crown relative height and shape parameter are defined as $\frac{h}{b} = 2$ and $\frac{b}{r} = 1$, respectively. This means that the tree crowns are modeled as spheres that are separated from the ground by half their diameter (Lucht et al., 2000). The statistical fitting of the model to observations requires several measurements. Therefore, both Aqua and Terra MODIS instruments deliver input to the inversion process (Strahler et al., 1999; Lucht et al., 2000). A back-up algorithm offers model inversions when only few observations are available. This algorithm makes use of the BRDF properties of previous full inversions and scales these shapes to new measurements. This allows inversions with as few as 3 observations. This back-up is termed magnitude inversion. However, the reliability of the inverted model suffers. The number of magnitude inversions rises with increasing cloud cover as fewer observations become available. This is often the case over tropical forests.

Observations of the influence of solar geometry on EVI are already available at low resolution (30 to 1 000 m) from satellites (Moura et al., 2012; Morton et al., 2014) and medium resolution (10 m) from plane (Galvão et al., 2011). An analysis on finer scales that could reveal processes that control EVI on the sub-crown level is still open. Hence, the first objective of this study was to investigate the dependence of EVI with sub-crown resolution. The first research question arising from this was:

RQ1 Does the solar geometry dependence of EVI persist on sub-crown scale?

As mentioned above the MCD43 product suite provides the possibility to model BRFs at given solar and viewing geometry. In this sense it provides an opportunity to filter solar and viewing geometry effects from observations. But for this application the product needs to be able to reproduce the EVI-solar geometry relationship found in observations. This provides the context for the second research question:

RQ2 Is the influence of solar geometry comparable between EVI derived from RTLSR modeled reflectances and observed EVI?

2 Methods

2.1 Fieldcampaign

The GRS Guyana field campaign in cooperation with the Guyana Forestry Commission in November 2014 offered unique opportunities to acquire data for this project. The target region was part of the Vaitarna Holdings Concession in Guyana (Figure 2.1). This area is located on the Guyana shield, which is characterized by tropical forest on nutrient poor, white sand. Dark colored rivers can be found in the closer surroundings, which point to high organic acid contents and hence low pH. Sandy soils with low pH have typically a low cation exchange capacity, which means that they can only hold low amounts of nutrients. These are conditions under which accelerated nutrient cycling takes place. From this result many ecological niches that lead to ecosystems rich in biodiversity.

One of the instruments that were part of the campaign was the hyperspectral mapping system (HYMSY) onboard an Altura PRO AT8 multicopter Unmanned Aerial Vehicle (UAV). The HYMSY consists of a pushbroom spectrometer with 328 pixels, a regular photo camera and a miniature GPS-Inertial Navigation System (INS). A processing chain, developed in the Laboratory of Geo-Information Science and Remote Sensing at Wageningen UR, transforms the datastreams from these instruments to co-registered RGB orthomosaics, Digital Surface Models (DSMs) and hyperspectral data cubes at fine spatial resolution (Suomalainen et al., 2014). For this the highly overlapping photos from the photo camera are processed with photogrammetric software to produce the orthomosaic and DSM. The DSM is then used to

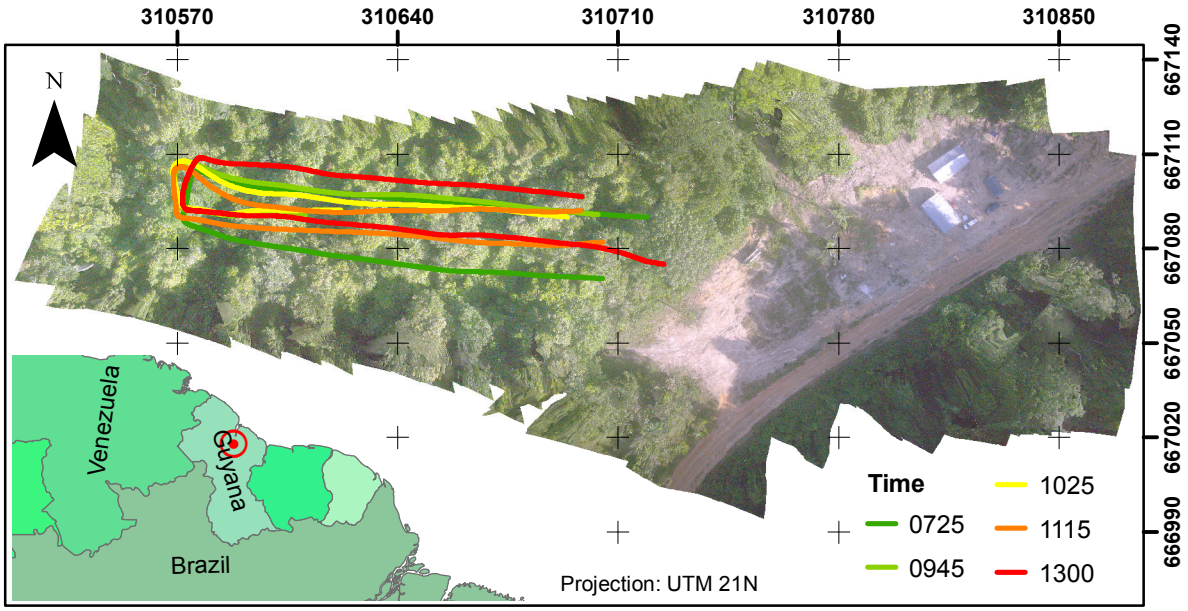

Figure 2.1: Study Area with clearing and field camp in the east. Flightpaths with active sampling are shown as colored lines. RGB image based on earliest flight orthomosaic acquired at $\theta_s = 64.5°$. Inset shows location of study area within Guyana as red point.

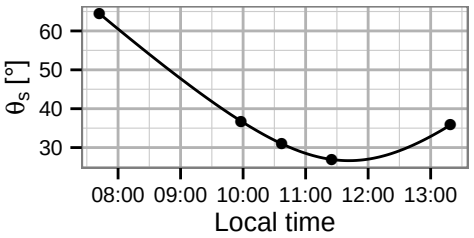

Figure 2.2: Course of θ_s for November 24, 2014 at N 6.031591° W 58.71199° (center point of the study site). The five flights are indicated as points.

determine the viewing geometry at the times when photos were taken. Since the hyperspectral line scanner has much higher acquisition speed than the photo camera, the orientations in between available photogrammetric orientations need to be interpolated. This is achieved with data from the GPS-INS. In this way high accuracy orientations and positions for each scan line can be determined. The geo-location for each pixel within a scan line is then identified with its position in the scan line and the knowledge that the spectrometer covers a field of view of 42.4°. The hyperspectral data is produced in 101 spectral bands ranging from 400 to 950 nm with 9 nm bandwidth (FWHM). A Spectralon 25% gray reference panel (Labsphere Inc) is used to calibrate the data for actual illumination conditions. The final datacube contains 328 cross-track pixels and covers a field of view of 42.4°.

The aim of the sampling design was to maximize the span of captured solar geometries. For the field campaign we chose to spread the samplings over the course of the morning, which covered the sun's lowest elevation angle until its angle at noon. The afternoons would have meant only repeated values of θ_s and tended to be cloudier. For fast repeated sampling in case of favorable weather conditions we selected the study area to be close to the base camp (Figure 2.1). During the flights the hyperspectral line scanner was steered in the direction of the sun to optimize sampling of the principal plane. The flight path target waypoints were kept constant for all flights, but different wind conditions and errors of the GPS receiver resulted in slightly deviating paths as seen in Figure 2.1. The 5 flights analyzed in this study were executed on November 24, 2014. The solar geometry of these flights can be seen in Figure 2.2.

The HYMSY data was processed per flight with the processing chain described above. Additionally, spectral reflectances were corrected for dependence of the reflectance panel on illumination geometry. For this the correction factors were assumed to be equal for all wavelengths and equal to available 99% reference panel correction factors. However, the spatial relationships in the HYMSY samplings were disregarded for the first part of this analysis. The hyperspectral pixels were rather treated as independent samples of the forest canopy. In this sense the HYMSY was considered a spectrometer with parallel acquisition capabilities and an acquisition speed of 8 200 samples per second. To gain more insight into spatial patterns the fully geo-rectified hyperspectral products were analyzed as well.

The solar geometry for each flight was calculated based on longitude and latitude of the study site (N 6.031591°, W 58.71199°), and the clock time when the UAV was halfway through the sampling procedure. With these parameters solar geometry could be calculated with the `sunAngle` function in the R `oce` package. This function is based on a National Aeronautics and Space Administration (NASA) FORTRAN code, which is turn is based on the *The Astronomical Almanac* (Michalsky, 1988).

2.2 Solar Geometry Dependence on Sub-Crown Scale

For the production of vegetation indices comparable to those acquired by MODIS, MODIS spectral bands were simulated with the hyperspectral datacubes. For this the hyperspectral bands were averaged as follows:

- blue: 460-480 nm (MODIS: 459-479 nm);
- red: 620-670 nm (MODIS: 620-670 nm);
- NIR: 840-875 nm (MODIS: 841-876 nm).

Additionally, the simulated bands' spectral response was assumed to approximate MODIS response curves. To assess the dependence of EVI on solar geometry while excluding viewing angle effects, only nadir viewing samples ($\theta_s \leq 5°$) were taken into account. Next to EVI, also NDVI was calculated because it shows only minor dependencies on view and solar angle effects (Sims et al., 2011). In this sense it served as a benchmark. The two indices are formulated as:

$$NDVI = \frac{\rho_{NIR} - \rho_{red}}{\rho_{NIR} + \rho_{red}} \tag{2.1}$$

$$EVI = 2.5 \times \frac{\rho_{NIR} - \rho_{red}}{\rho_{NIR} + 6\,\rho_{red} - 7.5\,\rho_{blue} + 1} \tag{2.2}$$

The solar geometry dependence was expressed in terms of a linear regression model:

$$VI_i = \beta_0 + \beta_1 \times \theta_{s,i} + \varepsilon_i \tag{2.3}$$

where VI_i is the vegetation index, β_0 and β_1 are parameters for the linear model, and ε_i are the residuals. The slope parameter β_1 characterizes the strength of the solar geometry dependence and has the unit $\frac{\Delta VI}{\Delta \theta_s}$. The significance of β_1 was an indicator for the influence of θ_s on EVI.

2.3 Solar Geometry Dependence in RTLSR Model

Besides assessing the EVI-solar geometry relationship with high resolution data, another question here was if the RTLSR model can reproduce this relationship. With the MODIS MCD43 product suite a vast database of useable model parameters is available. This database was exploited to acquire a pool of valid RTLSR model parameters tuples for the area around the UAV study site. One parameter tuple consists of the isotropic f_{iso}, volumetric f_{vol} and geometric f_{geo} parameter for each blue, red and NIR band, so in total 9 parameters. All pixels within a range of 5 km from the study site were extracted from MCD43A1 h12v08 MODIS tiles reaching from Dec 19, 2013 until Dec 27, 2014, making up a total of 48 tiles. The MCD43A1 product has a spatial resolution of approximately 500 m. Additionally, the inversion quality information was extracted from the MCD43A2 product. This quality information flags if a full or magnitude inversion were applied.

With each parameter tuple from this database the EVI-solar geometry relationship was analyzed by means of linear regression models. The regression model was the same as for the UAV data analysis (Eq. 2.3). EVI was modeled at discrete Solar Zenith Angles (SZAs) ranging from 0° to 60° in steps of 5° and with $\theta_v = 0$, meaning nadir viewing. As before the

slope parameter of the linear regression represented the EVI-solar geometry relationship. The significance of the slope parameter described if the linear approximation was suitable. The set of resulting slope parameters for analyzed in respect to their mean and distribution. Furthermore, the connection between the single kernel values and the EVI-solar geometry relationship as well as the impact of the inversion quality were investigated.

3 Results

3.1 Solar Geometry Dependence on Sub-Crown Scale

In total 231 547 spectral samples at nadir ($\theta_v \leq 5°$) with an approximate resolution of 0.2 m at the canopy level have been collected. The 5 single flights contributed 12.8% ($\theta_s = 64.5°$), 31.6% ($\theta_s = 36.8°$), 14.4% ($\theta_s = 35.8°$), 22.4% ($\theta_s = 31.0°$) and 18.8% ($\theta_s = 26.9°$) to the nadir samples. The average EVI decreased from 0.580 ($\theta_s = 26.9°$) to 0.436 ($\theta_s = 64.5°$) (Figure 3.1). The average response of EVI to θ_s, which correponds to β_1 in Eq. 2.3, was found to be -0.00285 $\frac{\Delta EVI}{\Delta \theta_s}$ ($p < 0.001$).

The linear model explained only few of the data's variance, as shown by the low r^2 of 0.036. This can be explained with the high spatial variance within the sample sets, which prevents a good fit of a linear model. The EVI variability within the sample sets expressed as standard deviation reached as much as 0.239 ($\theta_s = 64.5°$). Galvão et al. (2011) found EVI standard deviations of 0.02 and 0.09 for Hyperion and airborne Hymap imagery over seasonal evergreen tropical forest in Acre (Brazil). These two sensors have spatial resolutions of 30 m and 10 m, respectively. Despite the differences in study areas between Galvão et al. (2011) and this study, the trend of higher variance in EVI with higher resolutions becomes clear from these numbers. It can be explained with more diverse elements that make up individual pixels in higher resolution images, while these elements are averaged at lower resolutions. Particular low EVI values can stem from soil and dead plant material at the forest floor and shadowing effects within the canopy.

On the other hand, NDVI experienced a weaker and positive linear trend of +0.001 $\frac{\Delta NDVI}{\Delta \theta_s}$ ($p < 0.001$). The average NDVI ranged from 0.820 ($\theta_s = 26.9°$) to 0.870 ($\theta_s = 64.5°$). These high values are generally described as saturation over dense forests (Gao et al., 2000; Huete

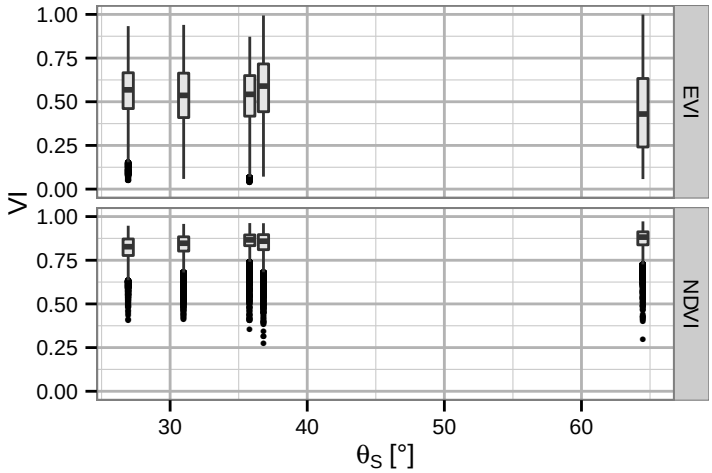

Figure 3.1: Boxplot of EVI and NDVI at four different θ_s, only pixels acquired with nadir viewing geometry ($\theta_v < 5°$) were taken into account. Boxes mark first, second and third quartiles. Points indicate outliers specified with Tukey's method.

et al., 2002). Concerning the explained variance, the NDVI linear model with an r^2 of 0.045 was comparably poor as the EVI model. But in contrast to EVI, NDVI showed much smaller variances with a maximum of 0.066 ($\theta_s = 26.9°$). This is in accordance with the saturation of NDVI over dense canopies. In this case it also points to low influence of shadowing on NDVI. Especially during the early morning flight with $\theta_s = 64.5°$ many parts of the canopy were shadowed, but NDVI was insensitive to them (Figure 2.1).

In contrast, EVI experienced an increase of variance with θ_s. The standard deviation increased from 0.154 ($\theta_s = 26.9°$) to 0.239 ($\theta_s = 64.5°$). This might well be explained by an impact of increasing within canopy shadowing with increasing θ_s. In this sense, shadowed canopy elements would show reduced EVI at higher θ_s, while illuminated elements would be stable; thus the overall variation would rise. The response of EVI to shadows is clear in both Figure 3.2 and 3.3. Especially during the early morning flight shadowed areas are large. The canopy elements facing East were illuminated and showed generally higher values of EVI. In contrast, the data collected at 11:25 local time resulted in much smaller shadowed areas. These observations were possible because of the high resolution of the imaging system and the canopy, that was open in places of abandoned skid trails resulting from logging activity in the study area.

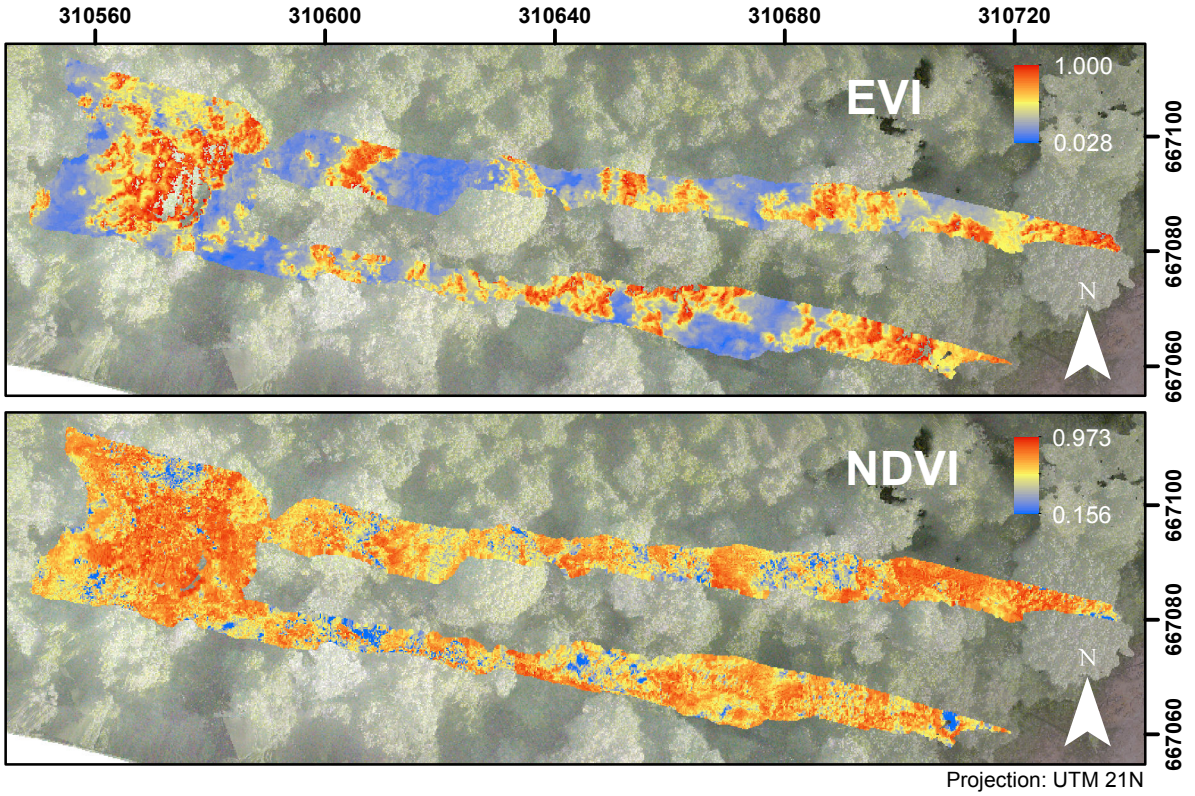

Figure 3.2: Georectified EVI and NDVI layers over orthomosaic for flight at 07:42 (Guyana time) ($\theta_s = 64.48°$). Orthomosaic has transparency and is underlaid with digital surface model to increase visibility of shadows.

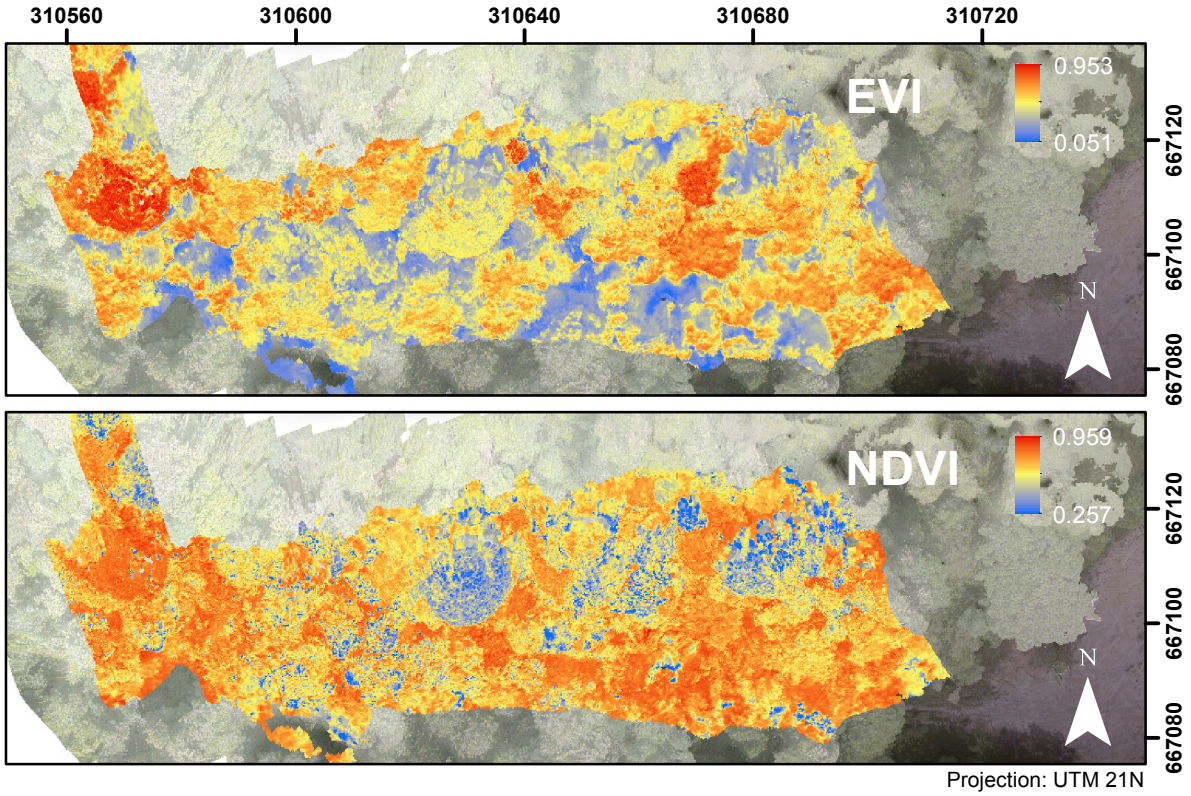

Figure 3.3: Same as 3.2, but for 11:25 (Guyana time) ($\theta_s = 31.0°$).

3.2 Solar Geometry Dependence in RTLSR Model

A total number of 13 307 kernel tuples was involved in the analysis of which 7.9% (1 047 tuples) stemmed from full inversions. The linear regression model proved to fit the EVI-solar geometry relationship well: for 96.2% of the tuples the model had an R^2 of more than 0.9. Moreover, EVI was significantly correlated with SZA in 98.8% (13 148) of all cases ($p < 0.01$). This shows the strong connection between EVI and solar geometry in the RTLSR model. The slope parameter was on average -0.00149 $\frac{\Delta EVI}{\Delta \theta_s}$. This relationship is about 2 times weaker compared to that one derived from the UAV. The NDVI correlation with θ_s was with +0.00034 $\frac{\Delta NDVI}{\Delta \theta_s}$ about 4.4 times smaller and with an opposite sign compared to the EVI relationship in the RTLSR model.

In general, the dependence on solar geometry stems from the different characteristic forms of the BRDFs when modelled with the RTLSR model. The EVI BRDF tends to have a cone shape and shows a strong hotspot effect, while the NDVI BRDF has a bowl shape without a hotspot (Figure 3.4). Additionally, NDVI is much more stable against viewing angle effects, which can be noted by the scale of the z-axes in Figure 3.4. A change of θ_s as seen in Figure 3.4 from 0° to 30° results in a much stronger reaction of EVI compared to NDVI. In this way, the RTLSR model generally reproduces the dependence of EVI on solar geometry.

The produced dataset of parameter tuples and derived slope parameters allowed also to investigate how the single kernel parameters are related to the slope parameter. Figure 3.5 summarizes these relationships. It can be noted that kernel parameters for the blue and red

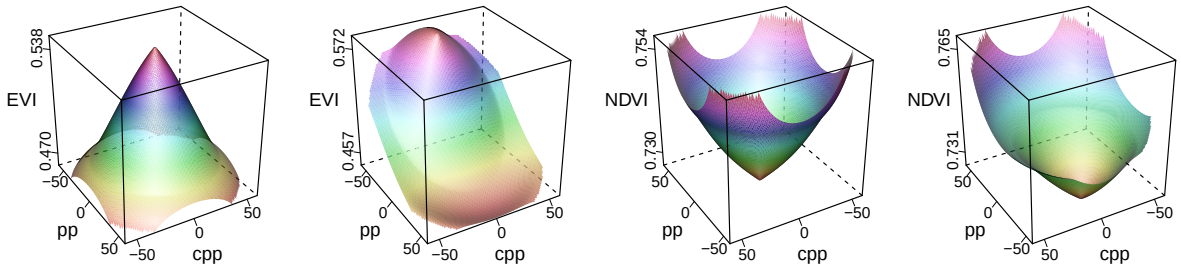

(a) EVI ($\theta_s = 0°$) **(b)** EVI ($\theta_s = 30°$) **(c)** NDVI ($\theta_s = 30°$) **(d)** NDVI ($\theta_s = 30°$)

Figure 3.4: RTLSR modeled EVI and NDVI as function of viewing geometry for $\theta_s = 0°$ and $\theta_s = 30°$. Underlying RTLSR kernel parameters are median kernel parameters based on all parameter tuples extracted from MODIS MCD43A1 as described in Section 2.3. Colors represent vegetation index values. Negative θ_v represent backscattering. Axes pp is principal plane, cpp is cross principal plane. Note the different observation angles between EVI and NDVI.

band were mostly indifferent to the slope parameter. This is in agreement with Galvão et al. (2011) and Samanta et al. (2012), who emphasize that EVI is strongly functionally dependent on NIR, so that the other bands becomes less influential. This in mind the NIR parameters showed medium to strong correlations with the slope parameter. Increasing values for the NIR isotropic parameter f_{iso}^{NIR} went along with a stronger dependence of EVI on the solar geometry. Based on the conclusions drawn in Section 3.1 this trend might be indirectly mediated by a higher number of bright crowns. These would not only raise the general scene brightness and thereby the isotropic parameter, but also the shadowing effects within the canopy. The same mechanism works in case of the NIR geometric parameter f_{geo}^{NIR}. As the geometric parameter represents shadowing effects within the canopy it most directly and strongly influences the dependence of EVI on the SZA: a more structural inhomogeneous canopy results in more shadows with higher θ_s. On the other hand, the NIR volumetric parameter f_{vol}^{NIR} was positively correlated with the slope parameter. This represents the opposite effect to shadowing, namely a denser canopy with fewer gaps and shadows. In such a case the canopy behaves more like the RossThick model which assumes a dense medium of randomly oriented reflecting facets. In line with the conclusions obtained with the UAV data in Section 3.1, the correlations in Figure 3.5 point out that the RTLSR model does not only reproduce the dependence of EVI on solar geometry, but also does this for the right reasons.

Apart from the general coherent behavior the RTLSR model showed irregular behavior in respect to two inversion quality levels. One such can be seen in Figure 3.5 for the f_{geo}^{NIR} parameter: while the full inversion followed a general linear model, the magnitude inversion parameters additionally clustered at around a value of 0.03 with indifferent behavior to the slope parameter. Assuming shadowing as the principal reason for the EVI-solar geometry dependence a constant shadowing parameter should not result in different slope parameters. Another irregularity appeared in case of the average slope parameter. Figure 3.6 shows histograms that summarize the derived slope parameters for EVI and NDVI in respect to the two inversion quality levels. Especially EVI slopes showed a strong convergence towards a central value for magnitude inversions of -0.00143 $\frac{\Delta EVI}{\Delta \theta_s}$. On the other hand, full inversions tended to be spread over a wider range. The full inversion slope values were in general also lower with a mean

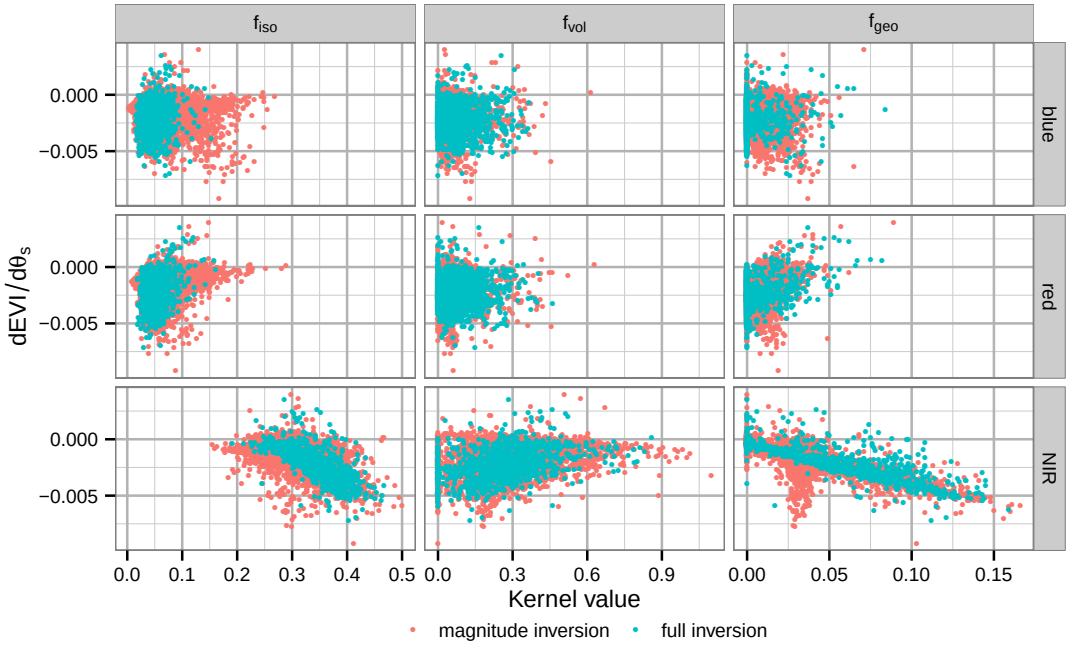

Figure 3.5: Scatterplots of $dEVI/d\theta_s$ against RTLSR kernel parameters.

of -0.00219 $\frac{\Delta EVI}{\Delta \theta_s}$, thereby coming closer to the slope derived from the UAV data. In case of NDVI the distributions of slopes for the two quality levels were closer to each other, but the mean of the parameters changed from positive (0.00038 $\frac{\Delta NDVI}{\Delta \theta_s}$) for magnitude to negative (-0.00014 $\frac{\Delta NDVI}{\Delta \theta_s}$) for full inversions. Even though the sample size for full inversions is much lower than for magnitude inversions, these results suggest a decreased ability of magnitude inversions to depict the correct EVI-solar geometry relationship.

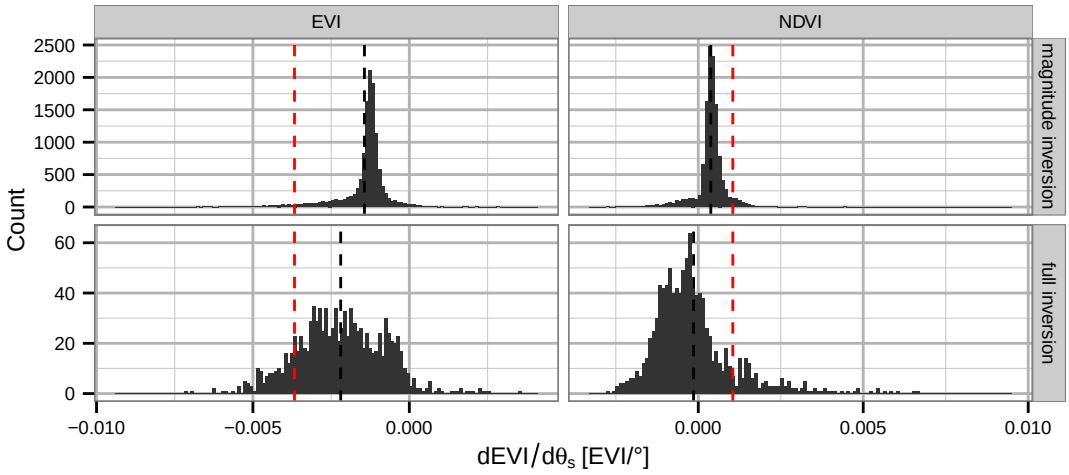

Figure 3.6: Histograms of $dEVI/d\theta_s$ for EVI and NDVI for full and magnitude inversions. Dashed black lines represent sample mean, dashed red lines represent mean from UAV observed data (Section 3.1).

4 Discussion & Conclusions

The EVI was extensively used for remote sensing based studies of the Amazon tropical forests. Recent studies point out the dependence of EVI on viewing and solar geometry, and thereby warn to be cautious in interpreting EVI time series data (Galvão et al., 2011; Sims et al., 2011; Moura et al., 2012). Morton et al. (2014) go further and claim that seasonal changes of canopy greenness expressed as EVI is solely an effect of the annually changing solar geometry. This study provides evidence that EVI of evergreen broadleaf tropical forest is dependent on solar geometry on sub-crown scale. This supports findings of previous studies (Galvão et al., 2011; Sims et al., 2011; Moura et al., 2012). Additionally, EVI as modeled with the RTLSR model was found to be dependent on solar geometry, but with about half the magnitude as found in direct observations with the UAV.

In particular, the hyperspectral mapping system (HYMSY) onboard the octocopter Altura PRO AT8 multicopter UAV proved useful to study effects of solar geometry on EVI. Its flexibility allowed observations at different daytimes to follow the course of the sun. The high number of bands allows flexible aggregation and simulation of multispectral sensors. This would also permit to test other indices. Furthermore, the data was recorded close to the Earth's surface so that atmospheric effects on the observations can be treated as neglible. Particular in this study the sub-crown resolution allowed the identification of processes that happen on the sub-pixel level of satellite data such as MODIS or Landsat.

For the evaluation of the magnitude of the EVI-solar geometry relationship, only few comparisons exist. As discussed in Chapter 1, only few studies investigated the relationship so far. Those do not state an explicit value in terms of $\frac{\Delta EVI}{\Delta \theta_s}$, but such values can be deduced from shown graphs. For instance, Moura et al. (2012) observed an EVI increase from 0.54 in June ($\theta_s = 43°$) to 0.60 in September ($\theta_s = 28°$), which corresponds to a trend of -0.004 $\frac{\Delta EVI}{\Delta \theta_s}$. This dependence is about 40% stronger than here, but also negative. Galvão et al. (2011) also investigated intra-annual EVI, but do not give exact solar geometries. Assuming an overpass time of 14:00 UTC, as taken from Terra Orbit Tracks[1], they observed an increase in EVI from 0.46 in June ($\theta_s = 42°$) to 0.58 in September ($\theta_s = 22°$) at their study site (S 12.79389°, W 51.65028°), which corresponds to a trend of -0.006 $\frac{\Delta EVI}{\Delta \theta_s}$. Of course, this evaluation is much coarser than for Moura et al. (2012), but points to the same trend. Still both studies show a stronger EVI-solar geometry relationships. One reason for this might have been a trend in canopy and air moisture content during the course of the UAV data acquisition. Another explanation might be actual changes in canopy spectral responses for Moura et al. (2012) and Galvão et al. (2011) since both studies were conducted in seasonal semideciduous forest. Nonetheless, Moura et al. (2012) argue that interannual variation across the same months in a year was random and low. In this sense the spectral response was mostly controlled by solar geometry effects.

The study of Galvão et al. (2011) also provides a reason for the sensitivity of EVI to solar geometry. Here it was found that EVI strongly reacts to canopy shadowing effects, which are controlled by solar geometry. Galvão et al. (2011) found a strong negative correlation between EVI and shade fraction, "a measure that varies with pixel brightness". This argumentation also agrees with the conclusions of Gao et al. (2000): They identified EVI as responsive to canopy

[1] http://www.ssec.wisc.edu/datacenter/terra/GLOBAL.html

structure, while NDVI is stronger related to chlorophyll content. Therefore, the dependence of EVI on structure is mediated through its sensitivity to shadows.

The RTLSR model as implemented in the MODIS MCD43 product suite represents a potential candidate to correct for viewing and solar geometry effects in EVI time series. However, the linear approximation of the dependence was found to be smaller than that of the UAV. This is not a problem of different resolutions: the slope parameter derived from Moura et al. (2012) was even smaller than the slope based on the UAV data, even though they used MISR images with 1.1 km spatial resolution. One reason for the divergence of the MCD43 product might be low differences in solar geometry during the 16 day acquisition period. Even though Aqua and Terra MODIS capture very different solar geometries because of their different overpass times, the variation within the 16 day acquisition period is only minor. Additionally, the MCD43 inversion quality had substantial impact not only on the EVI-solar geometry relationship, but also on the relationships among the RTLSR kernel parameters. This poses a severe problem for time series analysis of South American tropical forests if one wants to make use of the MCD43 product suite. Allowing only high quality inversions reduces the data availability to well below 10% of all periods. In this sense innovative BRDF modeling approaches are needed that can deal with low sampling density, which most likely involves more assumptions on the main drivers of the change in canopy spectral response (Vermote et al., 2009).

The principal motivation behind this study was to insvestigate the usability of the EVI for the study of tropical forests. It was found that EVI is strongly influenced by solar geometry compared to NDVI. This effect is mostly mediated through EVI's sensitivity to within canopy shadows. This supports Gao et al. (2000) who underline EVI's ability to characterize canopy structure additional to photosynthetic capacity. This is a good explanation for EVI's good performance in characterizing mid latitude forest functioning. Sims et al. (2011) even found better performance in deciduous than in evergreen sites, supporting the hypothesis that EVI can well describe canopy structural changes as found in deciduous forests. In case of deciduous forests canopy structure and carbon uptake are highly coupled over the year. Also tropical forests show this coupling (Doughty and Goulden, 2008). In this sense EVI appears to be a reasonable tool for its exploration. However, EVI is also sensitive to canopy chlorophyll content. This mixes the two domains, which is not optimal if the large scale coupling of structure and functioning is to evaluated. Therefore, characterization of tropical canopies with two indices – one structural, one chlorophyll sensitive – might be more helpful for further studies. As already stated NDVI proved strongly independent from solar geometry. Another option could be the Photochemical Reflectance Index (PRI) (Drolet et al., 2005). For the characterization of canopy structure indices based on RTLSR kernel parameters might filter more effectively on the structural signal (Gao et al., 2003; Chopping, 2008; Jiao et al., 2014).

Acknowledgements

The Guyana field campaign was supported by the SilvaCarbon and the ROBIN (Role of Biodiversity in Climate Change Mitigation) Projects. The author thanks Alvaro Lau Sarmiento and the Guyana Forestry Commission for the organisation. Further thanks go to Juha Suomalainen for his enthusiasm in conducting the field experiments and Mihai-Andrei Mirt for assistance during the experiments.

References

Anderson, L. O.: 2012, 'Biome-Scale Forest Properties in Amazonia Based on Field and Satellite Observations'. *Remote Sensing* **4**(12), 1245–1271.

Chopping, M. J.: 2008, 'Terrestrial Applications of Multiangle Remote Sensing'. In: S. Liang (ed.): *9th International Symposium on Physical Measurements and Signatures in Remote Sensing*. Dordrecht, pp. 95–144, Springer.

Doughty, C. E. and M. L. Goulden: 2008, 'Seasonal patterns of tropical forest leaf area index and CO2 exchange'. *Journal of Geophysical Research* **113**, G00B06.

Drolet, G. G., K. F. Huemmrich, F. G. Hall, E. M. Middleton, T. A. Black, A. G. Barr, and H. A. Margolis: 2005, 'A MODIS-derived photochemical reflectance index to detect inter-annual variations in the photosynthetic light-use efficiency of a boreal deciduous forest'. *Remote Sensing of Environment* **98**(2-3), 212–224.

Galvão, L. S., J. R. dos Santos, D. A. Roberts, F. M. Breunig, M. Toomey, and Y. M. de Moura: 2011, 'On intra-annual EVI variability in the dry season of tropical forest: A case study with MODIS and hyperspectral data'. *Remote Sensing of Environment* **115**(9), 2350–2359.

Gao, F., C. Schaaf, A. Strahler, Y. Jin, and X. Li: 2003, 'Detecting vegetation structure using a kernel-based BRDF model'. *Remote Sensing of Environment* **86**(2), 198–205.

Gao, X., A. R. Huete, W. Ni, and T. Miura: 2000, 'Optical-Biophysical Relationships of Vegetation Spectra without Background Contamination'. *Remote Sensing of Environment* **74**(3), 609–620.

Huete, A., K. Didan, T. Miura, E. Rodriguez, X. Gao, and L. Ferreira: 2002, 'Overview of the radiometric and biophysical performance of the MODIS vegetation indices'. *Remote Sensing of Environment* **83**(1-2), 195–213.

Huete, A. R., K. Didan, Y. E. Shimabukuro, P. Ratana, S. R. Saleska, L. R. Hutyra, W. Yang, R. R. Nemani, and R. Myneni: 2006, 'Amazon rainforests green-up with sunlight in dry season'. *Geophysical Research Letters* **33**(6), L06405.

Jiao, Z., M. J. Hill, C. B. Schaaf, H. Zhang, Z. Wang, and X. Li: 2014, 'An Anisotropic Flat Index (AFX) to derive BRDF archetypes from MODIS'. *Remote Sensing of Environment* **141**, 168–187.

Lorenz, K. and R. Lal: 2010, *Carbon Sequestration in Forest Ecosystems*, Vol. 2000. Dordrecht: Springer Netherlands.

Lucht, W., C. Schaaf, and A. Strahler: 2000, 'An algorithm for the retrieval of albedo from space using semiempirical BRDF models'. *IEEE Transactions on Geoscience and Remote Sensing* **38**(2), 977–998.

Michalsky, J.: 1988, 'The Astronomical Almanac's algorithm for approximate solar position (1950-2050)'. *Solar Energy* **40**, 227–235.

Morton, D. C., J. Nagol, C. C. Carabajal, J. Rosette, M. Palace, B. D. Cook, E. F. Vermote, D. J. Harding, and P. R. J. North: 2014, 'Amazon forests maintain consistent canopy structure and greenness during the dry season'. *Nature* **506**, 221–224.

Moura, Y. M., L. S. Galvão, J. R. dos Santos, D. A. Roberts, and F. M. Breunig: 2012, 'Use of MISR/Terra data to study intra- and inter-annual EVI variations in the dry season of tropical forest'. *Remote Sensing of Environment* **127**, 260–270.

Myneni, R. B., W. Yang, R. R. Nemani, A. R. Huete, R. E. Dickinson, Y. Knyazikhin, K. Didan, R. Fu, R. I. Negrón Juárez, S. S. Saatchi, H. Hashimoto, K. Ichii, N. V. Shabanov, B. Tan, P. Ratana, J. L. Privette, J. T. Morisette, E. F. Vermote, D. P. Roy, R. E. Wolfe, M. A. Friedl, S. W. Running, P. Votava, N. El-Saleous, S. Devadiga, Y. Su, and V. V. Salomonson: 2007, 'Large seasonal swings in leaf area of Amazon rainforests'. *Proceedings of the National Academy of Sciences of the United States of America* **104**(12), 4820–4823.

Nepstad, D. C., C. R. de Carvalho, E. A. Davidson, P. H. Jipp, P. A. Lefebvre, G. H. Negreiros, E. D. da Silva, T. A. Stone, S. E. Trumbore, and S. Vieira: 1994, 'The role of deep roots in the hydrological and carbon cycles of Amazonian forests and pastures'. *Nature* **372**(6507), 666–669.

Roujean, J.-L., M. Leroy, and P.-Y. Deschamps: 1992, 'A bidirectional reflectance model of the Earth's surface for the correction of remote sensing data'. *Journal of Geophysical Research* **97**(D18), 20455.

Saleska, S. R., S. D. Miller, D. M. Matross, M. L. Goulden, S. C. Wofsy, H. R. da Rocha, P. B. de Camargo, P. Crill, B. C. Daube, H. C. de Freitas, L. Hutyra, M. Keller, V. Kirchhoff, M. Menton, J. W. Munger, E. H. Pyle, A. H. Rice, and H. Silva: 2003, 'Carbon in Amazon forests: unexpected seasonal fluxes and disturbance-induced losses'. *Science* **302**(5650), 1554–1557.

Samanta, A., Y. Knyazikhin, L. Xu, R. E. Dickinson, R. Fu, M. H. Costa, S. S. Saatchi, R. R. Nemani, and R. B. Myneni: 2012, 'Seasonal changes in leaf area of Amazon forests from leaf flushing and abscission'. *Journal of Geophysical Research* **117**(G1), G01015.

Schaaf, C. B., F. Gao, A. H. Strahler, W. Lucht, X. Li, T. Tsang, N. C. Strugnell, X. Zhang, Y. Jin, J.-P. Muller, P. Lewis, M. Barnsley, P. Hobson, M. Disney, G. Roberts, M. Dunderdale, C. Doll, R. P. D'Entremont, B. Hu, S. Liang, J. L. Privette, and D. Roy: 2002, 'First operational BRDF, albedo nadir reflectance products from MODIS'. *Remote Sensing of Environment* **83**(1-2), 135–148.

Schaaf, C. B., J. Liu, F. Gao, and A. H. Strahler: 2011, 'Aqua and Terra MODIS albedo and reflectance anisotropy products'. In: B. Ramachandran, C. O. Justice, and M. J. Abrams (eds.): *Land Remote Sensing and Global Environmental Change – NASA's Earth Observing System and the Science of ASTER and MODIS*. New York, Dordrecht, Heidelberg, London: Springer, Chapt. 23, pp. 579–602.

Sims, D. A., A. F. Rahman, E. F. Vermote, and Z. Jiang: 2011, 'Seasonal and inter-annual variation in view angle effects on MODIS vegetation indices at three forest sites'. *Remote Sensing of Environment* **115**(12), 3112–3120.

Strahler, A. H., J.-P. Muller, and MODIS Science Team Members: 1999, 'MODIS BRDF/Albedo Product: Algorithm theoretical basis document version 5.0'. http://modis.gsfc.nasa.gov/data/atbd/atbd_mod09.pdf.

Suomalainen, J., N. Anders, S. Iqbal, G. Roerink, J. Franke, P. Wenting, D. Hünniger, H. Bartholomeus, R. Becker, and L. Kooistra: 2014, 'A Lightweight Hyperspectral Mapping System and Photogrammetric Processing Chain for Unmanned Aerial Vehicles'. *Remote Sensing* **6**(11), 11013–11030.

Vermote, E., C. Justice, and F.-M. Breon: 2009, 'Towards a Generalized Approach for Correction of the BRDF Effect in MODIS Directional Reflectances'. *IEEE Transactions on Geoscience and Remote Sensing* **47**(3), 898–908.

Xiao, X., S. Hagen, Q. Zhang, M. Keller, and B. Moore: 2006, 'Detecting leaf phenology of seasonally moist tropical forests in South America with multi-temporal MODIS images'. *Remote Sensing of Environment* **103**(4), 465–473.